Mon. Not. R. Astron. Soc. **000**, 000–000 (0000) Printed 1 February 2008 (MN LATEX style file v1.4)

APM z $\gtrsim$ 4 QSO Survey: Distribution and Evolution of High Column Density HI Absorbers

L. J. Storrie-Lombardi[1,2], M. J. Irwin[3], & R. G. McMahon[1]
[1] *Institute of Astronomy Madingley Road, Cambridge CB3 0HA, UK*
[2] *current address: Carnegie Observatories, 813 Santa Barbara Street, Pasadena, CA 91101 USA*
[3] *Royal Greenwich Observatory Madingley Rd, Cambridge CB3 0EZ, UK*
email: lisa@ociw.edu, mike@ast.cam.ac.uk, rgm@ast.cam.ac.uk

in press

1 February 2008

ABSTRACT

Eleven candidate damped Lyα absorption systems were identified in twenty-seven spectra of the quasars from the APM z $\gtrsim$ 4 survey covering the redshift range $2.8 \leq z_{absorption} \leq 4.4$ (8 with $z_{absorption} > 3.5$). High resolution echelle spectra (0.8Å FWHM) have been obtained for three quasars, including two of the highest redshift objects in the survey. Two damped systems have confirmed HI column densities of $N_{\rm HI} \geq 10^{20.3}$ atoms cm^{-2}, with a third falling just below this threshold. We have discovered the highest redshift damped Lyα absorber known at z=4.383 in QSO BR1202−0725.

The APM QSOs provide a substantial increase in the redshift path available for damped surveys for z>3. We combine this high redshift sample with other quasar samples covering the redshift range $0.008 < z < 4.7$ to study the redshift evolution and the column density distribution function for absorbers with log $N_{\rm HI} \geq$ 17.2. In the HI column density distribution $f(N) = kN^{-\beta}$ we find evidence for breaks in the power law, flattening for $17.2 \leq \log N_{\rm HI} \lesssim 21$ and steepening for $\log N_{\rm HI} > 21.2$. The breaks are more pronounced at higher redshift. The column density distribution function for the data with log $N_{\rm HI} \geq$20.3 is better fit with the form $f(N) = (f_*/N_*)(N/N_*)^{-\beta} exp(-N/N_*)$ with $\log N_* = 21.63 \pm 0.35$, $\beta = 1.48 \pm 0.30$, and $f_* = 1.77 \times 10^{-2}$. We have studied the evolution of the number density per unit redshift of the damped systems by fitting the sample with the customary power law $N(z) = N_0(1+z)^\gamma$. For a population with no intrinsic evolution in the product of the absorption cross-section and comoving spatial number density this will give $\gamma = 1/2$ ($\Omega = 1$) or $\gamma = 1$ ($\Omega = 0$). The best maximum likelihood fit for a single power law is $\gamma = 1.3 \pm 0.5$ and $N_0 = .04^{+.03}_{-.02}$, consistent with no intrinsic evolution even though the value of γ is also consistent with that found for the Lyman limit systems where evolution is detected at a significant level. However, redshift evolution is evident in the higher column density systems with an apparent decline in $N(z)$ for z>3.5.

Key words: cosmology—galaxies: evolution—galaxies: formation—quasars: absorption lines—quasars: individual (BR1033−0327, BRI1108−0747, BR1202−0725)

1 INTRODUCTION

This paper is the third of a series presenting results from studies of the QSOs discovered in the APM survey for z $\gtrsim$ 4 quasars. A study of the evolution of Lyman limit absorption systems over the redshift range $0.04 \leq z \leq 4.7$ was presented in Storrie-Lombardi et al. (1994) [Paper I]. The intermediate resolution (5Å) QSO spectra and the survey for high redshift damped Lyα absorbers are presented in Storrie-Lombardi et al. (1996) [Paper II]. The evolution of the cosmological mass density of neutral gas at high redshift and the implications for galaxy formation theories are discussed in Storrie-Lombardi, McMahon & Irwin (1996) [Paper IV]. In separate papers we will describe the intrinsic properties of the QSOs and studies of the Lyα forest clouds at high redshift. A high resolution study of the Lyα forest

region in a redshift $z = 4.5$ QSO has been completed by Williger et al. (1994).

How and when galaxies formed are questions at the forefront of work in observational cosmology. Absorption systems detected in quasar spectra provide the means to study galaxy formation and evolution up to redshifts of approximately five, back to when the Universe was less than 10 percent of its present age. Surveys for absorption features have several advantages over trying to directly detect galaxies at high redshift. Much shorter exposure times are required because the QSOs are relatively bright (R≈ 18-19.5) and the large equivalent width systems are easily detected in the spectra. This provides good absorption candidates to follow up with higher resolution spectra. The redshift and column density can be accurately determined from the wavelength of the absorption system and the line profile. This is far easier and more reliable than trying to directly get a spectrum of a very faint high redshift galaxy.

While the baryonic content of spiral galaxies that are observed in the present epoch is concentrated in stars, in the past this must have been in the form of gas. The principal gaseous component in spirals is neutral hydrogen which has led to surveys for absorbers detected by the damped Lyα lines they produce (Wolfe et al. 1986, hereafter WTSC; Lanzetta et al. 1991, hereafter LWTLMH; Lanzetta, Wolfe & Turnshek 1995, hereafter LWT; Wolfe et al. 1995; Paper II). Though damped Lyα systems are observationally very rare objects with ∼40 confirmed examples known, the HI mass per unit comoving volume they contain is roughly comparable to the mass density of baryonic matter in present-day spirals, ie. a major constituent of the Universe (Wolfe 1987, LWT). Their metal abundances are much lower than Galactic values (Pettini, Boksenberg & Hunstead 1990; Rauch et al. 1990; Pettini et al. 1994) and they are characterised by low molecular content and low, but not negligible, dust content (Fall, Pei & McMahon 1989; Pei, Fall & Bechtold 1991; Pettini et al. 1994), features consistent with an early phase of galactic evolution. They may be the progenitors of spiral galaxies like our own and are clearly important for the study of the formation and evolution of galaxies. They have been detected across a very large redshift range z≈[0.5,4.5] providing the means to pinpoint the epoch of formation of disk galaxies and study their evolution.

Eleven candidate damped Lyα absorption systems out of 32 measured Lyα features were identified in 27 spectra of the mainly non-BAL quasars from the APM z $\gtrsim$ 4 survey (Paper II). The eleven candidates cover the redshift range $2.8 \leq z_{absorption} \leq 4.4$ (8 with $z_{absorption} > 3.5$) and have estimated column densities $N_{\rm HI} \geq 10^{20.3}$ atoms cm^{-2}. In this paper the QSO BR1144−0723 with a candidate absorber at z=3.26 is removed from further consideration in the sample. It has been observed with the Anglo-Australian Telescope at high resolution and the damped candidate has been found to be all OVI absorption at z=4.0 (R. Hunstead, private communication). High resolution echelle spectra (0.8Å FWHM) were obtained by S. D'Odorico as part of the ESO key programme studying high redshift quasars for four of the QSOs in the APM sample (BRI0952−0115, BR1033−0327, BRI1108−0747, BR1202−0725). The signal-to-noise ratio in BRI0952−0115 was very poor but the other spectra have been used to confirm two Lyα features as damped with another falling just below the log $N_{\rm HI} \geq$ 20.3 threshold. We have discovered the highest redshift damped Lyα absorber known at z=4.383 in QSO BR1202−0725. The confirmation of the absorption systems is discussed in section 2. These data have been combined with data from previous surveys (WTSC, LWTLMH, and LWT) and the results for the Lyman limit systems obtained in Paper I to study the HI column density distribution for log$N_{\rm HI}$> 17.2 and redshift evolution of these systems for 0.008 < z < 4.7.

Numerous authors have studied the distribution of column densities, $f(N_{\rm HI})$, for Lyα absorption lines. The first determination was by Carswell et al. (1984) for lines with $10^{13} < N_{\rm HI} < 10^{16}$ atoms cm^{-2}. They found $f(N) \propto N^{-\beta}$ ($\beta = 1.7 \pm 0.1$). Damped Lyα absorption (DLA) systems comprise the high column density tail of neutral hydrogen absorbers with column densities of $N_{\rm HI} \geq 2 \times 10^{20}$ atoms cm^{-2}. They dominate the baryonic mass contributed by HI. When damped systems are included in the column density distribution function for a single power law fit the exponent is $\beta = 1.4$–1.7 (cf. Tytler 1987; Petitjean et al. 1993 and references therein). Assuming the baryonic mass is proportional to the HI column density and takes the form $f(N_{\rm HI}) \propto N^{-\beta}$ for the HI column density distribution function, the mass contribution from the damped systems can be estimated as

$$\begin{aligned} M_{total} &\propto \int_{N_1}^{N_2} N_{\rm HI} f(N_{\rm HI}) dN_{\rm HI} \\ &\propto \int_{N_1}^{N_2} N^{-\beta} N dN \qquad \text{(assume } \beta \neq 2\text{)} \\ &\propto \frac{1}{2-\beta}\Big[N_2^{2-\beta} - N_1^{2-\beta}\Big]. \end{aligned} \tag{1}$$

One problem with the power law representation is that if $\beta < 2$, as all current estimates indicate, then the total mass in damped systems diverges unless an upper bound to the HI column density is assumed. For example, if we take 20.3 $\lesssim$ log $N_{\rm HI}$ $\lesssim$ 22, the fractional contribution to the total HI mass for damped systems, M_f, is then $M_f = 0.86$ for $\beta = 1.5$ and $M_f = 0.69$ for $\beta = 1.7$. However, there is no a priori reason for assuming this upper limit and hence there is no strict upper bound to any estimate of the total HI mass in damped systems. An alternative parameterisation using a gamma function to describe the HI column density distribution was adopted by Pei & Fall (1995) and provides an elegant solution to the diverging mass problem. We discuss these points in more detail in section 3 and the redshift evolution of the absorbers in section 4.

2 CONFIRMATION OF DAMPED Lyα SYSTEMS

2.1 Echelle Observations

Echelle spectra of four QSOs were obtained in March, 1993 by S. D'Odorico as part of an ESO key programme studying high redshift quasars. They were taken at La Silla with the 3.5m NTT telescope using the EMMI instrument in echelle mode using a 2048×2048 pixel LORAL CCD as the detector. A slit of 15" in length was used and generally the slit width

Table 1. ESO Observations March, 1993

QSO	Date (UT)	Exp (secs)	Grating	Slit (")
BRI0952 − 0115	93 Mar 14	5400	GR9CD3	1.2
	93 Mar 14	7200	GR9CD3	2.0
BR 1033 − 0327	93 Mar 15	7200, 8000	GR9CD3	1.2
BRI1108 − 0747	93 Mar 15	6000	GR9CD3	1.2
	93 Mar 15	6000	GR9CD4	1.2
BR 1202 − 0725	93 Mar 14	8000	GR9CD3	1.2
	93 Mar 15	6797	GR9CD3	1.2
	93 Mar 15	7200, 8000	GR9CD4	1.2

was 1.2". Two grating setups were used, one covering 4700-8300Å and the other covering 5800-9500Å with a resolution of ∼40 km s^{-1} (1Å). [See Giallongo et al. 1994 for more details.] The observations are summarised in table 1.

The spectra were extracted and calibrated using the OPTEXT routines* in conjunction with IRAF. The final flux calibrated spectra agreed well with the existing 5Å spectra (Paper II) except in the case of BRI0952−0115 where the signal-to-noise ratio was very poor and the relative flux different by a factor of two. This spectrum has been excluded from further analysis. Though not of exceedingly high quality the spectra were suitable for fitting the damped Lyα candidates.

2.2 Fitting the Damped Candidates

The damped candidate system profiles were fit using the **vpgti**† Voigt profile fitting software. The programme requires three input spectra: the object, the errors, and the continuum. The OPTEXT routines used in the reduction created the first two and the continuum spectra were created by using continuum fits for the WHT spectra (Paper II) and extrapolating them to the echelle spectra as was done in Williger et al. 1994. The centroids of the Lyα features were determined from narrow metal lines (e.g. OI, CII) and then the Lyα lines were fit in a region 50-100Å around the candidate feature. Generally, candidate damped systems seen in the low resolution spectra appeared much stronger than they actually are, due to blending of the dense Lya forest lines at low resolution. In all three QSOs the candidate damped systems are seen at higher resolution to break up into multiple overlapping components. The complexity of the blend coupled with residual uncertainty in the exact placing of the continuum level causes some of the error estimates from VPFIT to be somewhat optimistic. In particular for BRI1108−0747 and BR1202−0725 numerical simulations suggest an error in log $N_{\rm HI}$ of $\sigma = 0.15$ should be adopted. The fitted lines are summarised in table 2.

a) BR1033−0327, (z_{em} = 4.509, $z_{absorption}$ = 4.15) The absorption candidate at z=4.15 had been previously studied (Williger et al. 1994) with a 12 km s^{-1} echelle spectrum taken at CTIO. Their spectrum covered only the blue wing of the system and from this the column density was estimated to be no greater than 3×10^{20} atoms cm^{-1}. With spectral coverage of the entire absorber it is seen to be a complex system of at least 5 absorbers with a total column density of log $N_{\rm HI}$= 20.15 ± 0.11 atoms cm^{-2} (1.4×10^{20}). In Paper II the column density was estimated to be log $N_{\rm HI}$= 20.2. The redshifts of the Lyα absorbers were determined from 5 tentatively identified OI1302 lines in the CTIO spectrum. The signal-to-noise ratio in the order where the Lyβ lines lie was too low to use in the fit. The spectrum with the best fit line profiles and $\pm1\sigma$ fits are shown as solid lines in figure 1(a). The error array and normalised continuum are shown as dotted and dashed lines, respectively. The small spike at ≈6270Å is real. It also appears in the 5Å resolution spectrum (Paper II).

Table 2. Lyman-α Absorption Systems

QSO	Absorption Redshift	log $N_{\rm HI}$
BR1033 − 0327	4.14945	19.80 ± 0.10
	4.15314	18.69 ± 0.30
	4.16647	19.70 ± 0.15
	4.16726	19.37 ± 0.42
	4.17481	19.60 ± 0.24
BRI1108 − 0747	3.60673	20.33 ± 0.15
BR1202 − 0725	4.38290	20.49 ± 0.15

b) BRI1108−0747, (z_{em} = 3.922, z_{dla} = 3.607) The absorber at z=3.61 is barely damped with a column density of log $N_{\rm HI}$= 20.33 ± 0.15 atoms cm^{-2}. In Paper II we estimated the column density to be log $N_{\rm HI}$= 20.2, so this system was not originally in the statistical sample. Several of the absorbers in the survey in Paper II have estimated column densities near the statistical sample threshold of log $N_{\rm HI}$= 20.3. We expect some to be confirmed above this value and some below. The profile fit and $\pm1\sigma$ fits are shown in figure 1(b). The redshift centroid was determined from a single strong CII1334 line.

c) BR1202−0725, (z_{em} = 4.694, z_{dla} = 4.383) The damped system in this QSO has a column density of log $N_{\rm HI}$= 20.49 ± 0.15. It is the highest redshift damped Lyα system known. The ESO spectrum is shown with the profile fit and $\pm1\sigma$ fits in figure 1(c). It was also measured in a higher resolution spectrum taken at CTIO (Wampler et al. 1996), and includes over 10 components. Lu et al. (1996) have observed it at Keck with HIRES and measure a column density of log $N_{\rm HI}$= 20.6 ± 0.1. It was estimated in Paper II to have a column density of log $N_{\rm HI}$= 20.5. The status of the systems detected in the APM Damped Lyα absorption survey is summarised in table 3. (It is an updated version of table 7 from paper II.) Those marked with an asterisk have column densities log $N_{\rm HI} \geq$ 20.3 atoms cm^{-2} and make up the statistical sample of high redshift absorbers used in the analysis. In Paper IV this data set is combined with previous surveys to study the evolution of the cosmological mass density of neutral gas at high redshift and the implications for galaxy formation theories are discussed.

* These were written by Bob Carswell, Jack Baldwin, and Gerry Williger for the reduction of CTIO echelle data.

† Written by R.F. Carswell, J.K. Webb, A.J. Cooke, and M.J. Irwin, see also Cooke (1994).

Table 3. Status of Absorbers in APM Damped Lyman-α Absorption Survey

QSO	z_{min}	z_{max}	z_{em}	z_{dla}	W_{rest} Å	log N_{HI} estimate	log N_{HI} actual
BR 0019 − 1522	2.97	4.473	4.528	3.42	7.6	20.0	
				3.98	12.3	*20.5	
				4.28	8.0	20.1	
BRI0103 + 0032	2.87	4.383	4.437	4.23	5.8	19.8	
BRI0151 − 0025	2.74	4.142	4.194				
BRI0241 − 0146	2.86	4.002	4.053	3.41	5.7	19.8	
BR 0245 − 0608	2.96	4.186	4.238				
BR 0351 − 1034	3.09	4.297	4.351	3.62	6.6	19.9	
				4.14	6.3	19.9	
BR 0401 − 1711	2.82	4.184	4.236				
BR 0951 − 0450	2.93	4.315	4.369	3.84	24.0	*21.0	
				4.20	10.6	*20.3	
BRI0952 − 0115	2.99	4.372	4.426	4.01	18.0	*20.8	
BRI1013 + 0035	2.61	4.351	4.405	3.10	17.5	*20.8	
				3.73	9.6	20.2	
				4.15	7.4	20.0	
BR 1033 − 0327	2.91	4.454	4.509	4.15	9.6	20.2	20.15 ± 0.11
BRI1050 − 0000	2.83	4.233	4.286				
BRI1108 − 0747	2.64	3.873	3.922	2.79	8.3	20.1	
				3.607	9.0	20.2	*20.33 ± 0.15
BRI1110 + 0106	2.58	3.869	3.918	3.25	5.2	19.7	
				3.28	6.2	19.9	
BRI1114 − 0822	3.19	4.440	4.495	3.91	6.7	19.9	
				4.25	11.7	*20.4	
				4.45	5.3	19.7	
BR 1144 − 0723	Removed from sample.						
BR 1202 − 0725	3.16	4.637	4.694	3.20	5.4	19.7	
				3.38	7.1	20.0	
				4.13	7.8	20.1	
				4.383	13.2	20.5	*20.49 ± 0.15
BRI1328 − 0433	2.24	4.165	4.217	3.08	8.3	20.1	
BRI1335 − 0417	3.08	4.342	4.396				
BRI1346 − 0322	2.65	3.942	3.992	3.15	6.8	19.9	
				3.36	5.0	19.7	
				3.73	10.0	*20.3	
BRI1500 + 0824	2.39	3.894	3.943	2.80	11.3	*20.4	
GB 1508 + 5714	2.73	4.230	4.283				
MG 1557 + 0313	2.66	3.842	3.891				
GB 1745 + 6227	2.47	3.852	3.901				
BR 2212 − 1626	2.69	3.940	3.990				
BR 2237 − 0607	2.96	4.502	4.558	4.08	11.5	*20.4	
BR 2248 − 1242	2.94	4.109	4.161				

* These absorbers are above the statistical sample threshold of $N_{HI} \geq 2 \times 10^{20}$ atoms cm^{-2}.
z_{min} = minimum redshift at which a DLA could be observed
z_{em} = emission redshift of the QSO
z_{max} = 3000 km s^{-1} blueward of z_{em}
z_{dla} = redshift at which a damped candidate was observed

3 THE HI COLUMN DENSITY DISTRIBUTION FOR LOG $N_{HI} > 17.2$

3.1 Background

The distribution of the HI column densities for QSO absorption line systems has been investigated by several authors. Tytler (1987) found that the distribution may be represented by a single power law $f(N) \propto N^{-\beta}$ over the range $13.3 \leq \log N_{\rm HI} \leq 21.8$ with $\beta = 1.51 \pm 0.02$. He argued that this was evidence for a single population. Fitting the higher and lower column density systems separately, Tytler found $\beta = 1.61 \pm 0.10$ for $\log N_{\rm HI} < 16.7$ and $\beta = 1.35 \pm 0.07$ for $\log N_{\rm HI} > 17.2$, very similar slopes particularly considering the inadequacies of the data set. Sargent et al. (1980) argued that the forest lines and higher column density metal absorbers were distinct populations due to their different clustering properties. Sargent, Steidel & Boksenberg (1989) found a single power law fit the over the entire column density range but noted that since little detailed data was available for $15.5 \leq \log N_{\rm HI} \leq 17.2$, the region where the HI becomes optically thick, that this was not evidence for a single population. They also found $\beta = 1.39$ for $\log N_{\rm HI} \geq 17.3$. LWTLMH found the best fit for the high column density data ($17.2 \leq \log N_{\rm HI} \leq 21.8$) gave $\beta = 1.25$. All of these values for β agree within the errors. Petitjean et al. (1993) reviewed these results and concluded that neither a single nor double power fit well for $13.3 \leq N_{\rm HI} \leq 21.8$ but that there clearly was a flattening of the distribution function around $\log N_{\rm HI} \approx 16$.

Looking at the damped Lyα systems alone ($20.3 \leq \log N_{\rm HI} \leq 21.8$) LWTLMH found $\beta = 1.73$. Most of these investigators find no evidence for any substantial redshift evolution in the distribution function though LWT find an increased number of the highest column density systems at high redshift. Into this quagmire we wade with the absorption systems from the APM Damped Lyα Survey [Paper II] and the results for the Lyman-limit system evolution from Paper I to attempt to better quantify what is happening with the high column density HI at high redshift.

3.2 A Power Law Distribution Function

The form of the power law column density distribution function $f(N)$ typically used is

$$f(N) = kN^{-\beta}. \tag{2}$$

$f(N)dNdX$ is defined as the number of absorbers in an absorption distance interval dX with HI column density N in the range $N + dN$. The absorption distance X is used to remove the redshift dependence in the sample and put everything on a comoving coordinate scale since $\Delta z = 0.5$ at redshift 2 is not the same at as a $\Delta z = 0.5$ at redshift 4. If the population of absorbers is nonevolving (i.e. their number density multiplied by their cross-section does not change with redshift), the absorption distance can be defined as

$$X(z) = \int_0^z = (1+z)(1+2q_0 z)^{-1/2} dz, \tag{3}$$

therefore

$$X(z) = \begin{cases} \frac{2}{3}[(1+z)^{3/2} - 1] & \text{if } q_0 = 0.5; \\ \frac{1}{2}[(1+z)^2 - 1] & \text{if } q_0 = 0. \end{cases} \tag{4}$$

Table 4. Redshift and Absorption Distance Paths

Data Set	Δz	ΔX ($q_0 = 0$)	ΔX ($q_0 = 0.5$)
$0 < z < 4.7$			
APM Damped Lyα Survey	36.1	162.3	76.5
WTSC + LWTLMH + LWT	203.4	602.1	344.8
Combined	239.5	764.4	421.3
$z > 3$			
APM Damped Lyα Survey	30.5	141.2	65.5
WTSC + LWTLMH + LWT	13.0	54.6	26.7
Combined	43.5	195.8	92.2

(Bahcall & Peebles 1969; cf. Tytler 1987). The value of q_0 has little effect on the slope of the column density distribution function. In the analysis below we have utilised $q_0 = 0.5$. To allow for redshift evolution, the distribution function is normally generalised as

$$f(N, z) = kN^{-\beta}(1+z)^{\gamma}. \tag{5}$$

The damped Lyα systems and candidates from the APM survey shown in table 3 have been combined with previous surveys for damped Lyα systems (WTSC, LWTLMH, LWT) which results in a data set of 366 QSOs yielding 44 damped systems with $\log N_{\rm HI} \geq 20.3$ covering the redshift range $0.2 \leq z \leq 4.4$. The total redshift path and absorption distance covered by the surveys is shown in table 4. A maximum likelihood technique, described in Appendix A, has been employed to find values for β and k to determine if a power law fit describes the HI column density distribution for this sample. As already indicated a disadvantage of a power law model for the HI column density distribution of damped Lyα absorbers, is the divergent nature of the integral mass contained in the systems. Since it is straightforward to generalise the maximum likelihood method to alternative forms of the distribution, we explore in section 3.6 an alternative parameterisation based on a gamma distribution (cf. Pei & Fall 1995).

3.3 Results for a Single Power Law

A single power law fit to the combined data set described above of the form in equation 5 with $q_0 = 0.5$ results in $\beta = 1.74 \pm 0.12$ and $\log k = 13.9 \pm 2.3$ with similar values for $q_0 = 0$ ($\beta = 1.75, \log k = 13.9$). The quoted error for the normalisation constant k is large because for a small change in the value of β, k can change by 2 orders of magnitude. These results are in good agreement with the results found by LWTLMH ($\beta = 1.73 \pm 0.29$, log k$= 13.63 \pm 0.09$) and are plotted for the entire data set in figure 2. The data is binned for display purposes only with the vertical error bars plotted at the mean column density for each bin. We will see in the next section that a single power law is not a good fit to the data.

3.4 Cumulative HI Distribution

As shown in Paper I for the Lyman-limit system evolution, the arbitrary binning of the data for presentation in differential plots includes a subjective component that can mask

exactly what is happening in the underlying data. A cumulative distribution plot is far better at revealing the true nature of the distribution and this approach is examined now. The log of the cumulative number of damped Lyα systems detected versus log $N_{\rm HI}$ is plotted in figure 3(a). A point for the expected number of Lyman-limit systems that would be detected down to log $N_{\rm HI}$= 17.2 is shown with a circled star. This is calculated by integrating the number density per unit redshift ($N(z) = 0.27(1+z)^{1.55}$) over the redshift path covered by the n QSOs in the DLA sample, i.e.

$$\begin{aligned} {\rm LLS}_{expected} &= \sum_{i=1}^{n} \int N(z)dz = \sum_{i=1}^{n} \int_{z_{min}}^{z_{em}} N_0(1+z)^{\gamma} dz \\ &= \sum_{i=1}^{n} \int_{z_{min}}^{z_{em}} 0.27(1+z)^{1.55} dz. \end{aligned} \quad (6)$$

It is obvious from figure 3(a) that a power law will not fit the entire column density range 17.2 $\leq$ log $N_{\rm HI}\leq$ 22. A Kolmogorov-Smirnov (K-S) yields a probability of less than 10^{-7} that the fit represents the underlying data set. In figures 3(b-d) the same distribution is overplotted with single power law fits for different values of β that were fit to the graph by eye. (b) shows that $\beta = 1.34$ will fit from the Lyman limit column density through the damped systems with log $N_{\rm HI}\approx$ 21, a flatter slope than the canonical 1.5-1.7 range. (c) shows that $\beta = 1.69$ fits the damped distribution with 20.3 $\leq$ log $N_{\rm HI}\leq$ 21.2 well but does not describe the high or low column density tails of the distribution. (d) shows a fit to the sharp drop off in numbers for damped systems with log $N_{\rm HI} \gtrsim$ 21.3. This can be expected from looking at the estimated column densities for the damped systems in table 3 or by looking at the spectra. There are not a lot of heavily damped systems. Clearly the results for a single power law fit depend critically on the range of column densities included. This characteristic can explain much of the variation in the results previously seen by various authors that were summarised in section 3.1.

3.5 Redshift Evolution for 0.008 < z < 4.7

To qualitatively study the redshift evolution of the column density distribution of the damped Lyα systems the cumulative distribution shown in figure 3 has been split in half at redshift 2.5 and each set plotted individually (figure 4). The damped Lyα systems with $z > 2.5$ are shown by the solid line and the absorbers with $z < 2.5$ are shown by the dashed line. The higher redshift absorbers appear to have a slightly flatter slope up to log $N_{\rm HI}$=21 and then a sharper drop in the number of very high column density systems, though a K-S test shows that this is not a statistically significant difference. The evolution with redshift in the slope of the column density distribution is also apparent when looking at the differential $f(N)$. LWT plotted this in 3 redshift bins z=[0.008,1.5],[1.5,2.5], and [2.5,3.5]. In the highest redshift bin there was a flattening of the column density distribution slope towards higher column densities. In figure 5 we have plotted our combined data set with this same binning with the addition of one higher redshift bin z=[3.5,4.7]. The flattening of the distribution function towards higher column density systems in the z=[2.5,3.5] bin in the LWT data is no longer pronounced. The most striking feature is the steepness of the distribution in the highest redshift bin. It is not just steeper due to a decrease in the highest column density systems (log $N_{\rm HI}$>21), but there is also an increase in the number of lower column density systems relative to the other bins. Even if 15-20% of the candidate systems with log $N_{\rm HI}\approx$20.3 turn out not to be damped when observed at higher resolution, as we expect, this result still holds.

3.6 Results for a Gamma-Distribution

There are two strong motivating factors to find an alternative model for describing the HI column density distribution. First, as shown in section 3.4, there is direct evidence for an apparent variation in the power law slope as a function of $N_{\rm HI}$. This implies that a higher order functional form other than a power law is needed to describe the column density distribution. Second, as noted in the introduction, with a power law model the integral mass contained within damped Lyα systems is divergent for realistic values of β. This in turn means that it is impossible to assign a formal upper limit to any estimate of the neutral gas content of the early Universe. Consequently, following Pei and Fall (1995), we have chosen to model the data with a gamma distribution of the form

$$f(N,z) = (f_*/N_*)(N/N_*)^{-\beta} e^{-N/N_*} \quad (7)$$

where f_* is the characteristic number of absorbing systems at the column density N_*, and N_* is a parameter defining the turnover, or 'knee', in the number distribution. Both f_* and N_* may in general vary with redshift but for the moment we treat them as constants. This functional form is similar to the Schechter luminosity function (Schechter 1976). For $N << N_*$ the gamma function tends to the same form as the single power law, $f(N) \propto N^{-\beta}$; whilst for $N \gtrsim N_*$, the exponential term begins to dominate.

We can understand how a gamma function might provide a better description of the damped Lyα data by considering the differential logarithmic slope which is given by

$$\frac{dlogf(N,z)}{dlogN} = -\beta - \frac{N}{N_*} \quad (8)$$

As the column density approaches N_* the slope begins to steepen and rapidly turns over at higher column densities, qualitatively similar to what we observe in figures 3 and 4. Furthermore, the integral HI over the column density distribution (cf. equation 1) for $N_{min} << N_*$ is now given by $f_* N_* \tau(2-\gamma)$ where τ denotes the standard gamma function. This function is bounded if $\gamma < 2$.

The maximum likelihood technique outlined in Appendix A can readily be modified to incorporate this form. We note that the likelihood solution can be found over a two-dimensional grid of pairs of values of N_* and β, since the constant f_* can be directly computed using the constraint

$$m = \sum_{i=1}^{n} f_* \int_{N_{min}}^{N_{max}} \int_{z^i_{min}}^{z^i_{max}} f(N,z) dz dN \quad (9)$$

where m is the total number of observed systems. This is computationally much less intensive than doing a 3-D grid

search. The results of a single functional fit to the entire dataset are log $N_* = 21.63 \pm 0.35$, $\beta = 1.48 \pm 0.30$, and $f_* = 1.77 \times 10^{-2}$. The log-likelihood function results with confidence contours are shown in figure 6(a). The best fit is overplotted on the differential form of $f(N)$ in figure 6(b) and on the cumulative distribution in figure 6(c). (The single power law form of $f(N)$ was shown fitted to the same data in figures 2 and 3). The differential form of the plots (figures 2 and 6(b)) show little difference between the single power law and Γ-distribution fits. When displayed with the cumulative number of absorbers in figure 6(c), the Γ-distribution now clearly fits the entire data set with column densities log $N_{\rm HI} \geq$ 20.3. If the expected number of Lyman-limit systems are included in the fit, the results are log $N_* = 21.36 \pm 0.15$, $\beta = 1.16 \pm 0.15$, and $f_* = 4.43 \times 10^{-2}$. This also provides a reasonable fit to the data as shown in figure 7(a-c).

4 NUMBER DENSITY EVOLUTION WITH REDSHIFT

Differential evolution in the number density of damped Lyα absorbers has been described by LWT and Wolfe et al. (1995). While the change in number density per unit redshift is consistent with no intrinsic evolution of the absorbers over the range 0 < z < 3.5, they find that the systems with log $N_{\rm HI}$> 21 disappear at a much faster rate from z=3.5 to z=0 than does the population of damped absorbers as a whole. We now examine the redshift evolution of the damped Lyα absorbers in our combined data set by determining the number density of absorbers per unit redshift, $dN/dz \equiv N(z)$. In a standard Friedmann Universe for absorbers with cross section $\pi {R_0}^2$ and number density Φ_0 per unit comoving volume

$$N(z) = \Phi_0 \pi {R_0}^2 c H_0^{-1} (1+z)(1+2q_0 z)^{-1/2}. \quad (10)$$

It is customary to represent the number density as a power law of the form

$$N(z) = N_0 (1+z)^{\gamma}, \quad (11)$$

where $N_0 = \Phi_0 \pi {R_0}^2 c H_0^{-1}$. This yields $\gamma = 1$ for $q_0 = 0$ and $\gamma = 1/2$ for $q_0 = 1/2$ for the case of no evolution with redshift in the product of the number density and cross section of the absorbers (Sargent et al. 1980).

A maximum likelihood fit to the data yields $N(z) = 0.04(1+z)^{1.3 \pm 0.5}$ which is consistent with no intrinsic evolution even though the value of γ is similar to that found for the Lyman limit systems where evolution is detected at a significant level (Paper I; Stengler-Larrea et al. 1995). The log-likelihood function for γ and N_0 with >68.3% and >95.5% confidence contours is plotted in figure 8. We also find redshift evolution in the higher column density systems but with a decline in $N(z)$ for z>3.5. These results are displayed in figure 9. The entire data set is plotted as dashed lines with the above fit. The results for only the absorbers with log N(HI)≥ 21 are shown as solid lines. Figure 10 shows HI column density versus redshift, and the paucity of absorbers with log $N_{\rm HI}$> 21 at z > 4 is apparent.

5 CONCLUSIONS

Three QSOs from APM survey have been observed at 0.8Å resolution. Two have damped systems with confirmed HI column densities of $N_{\rm HI} \geq 10^{20.3}$ atoms cm^{-2}, with a third absorber falling just below this threshold. We have discovered the highest redshift damped Lyα absorber known at z=4.383 in QSO BR1202−0725. The two systems with $N_{\rm HI} \geq 10^{20.3}$ atoms cm^{-2}, and remaining nine candidate damped absorbers from the APM survey have been combined with data from previous surveys to study the column density distribution and number density evolution for absorbers with $N_{\rm HI} \geq 17.2$. If the HI column density distribution function is fit with a power law, $f(N) = kN^{-\beta}$, we find evidence for breaks in the power law, flattening for $17.2 \leq \log N_{\rm HI} \lesssim 21$ and steepening for $\log N_{\rm HI} \gtrsim 21.2$. The column density distribution function for the data with log$N_{\rm HI}$≥20.3 is better fit with the Γ-distribution form $f(N) = (f_*/N_*)(N/N_*)^{-\beta} exp(-N/N_*)$ with log $N_* = 21.63 \pm 0.35$, $\beta = 1.48 \pm 0.30$, and $f_* = 1.77 \times 10^{-2}$.

For the number density evolution of the damped absorbers (log $N_{\rm HI} \geq 20.3$) over the redshift range 0.008 < z < 4.7 we find the best fit of a single power law form for $N(z) = N_0(1+z)^{\gamma}$ yields $\gamma = 1.3 \pm 0.5$ and $N_0 = .04^{+.03}_{-.02}$. This is consistent with no intrinsic evolution in the absorbers even though the value of γ is similar to that found for the Lyman limit systems where evolution is detected at a significant level. Evolution is evident in the highest column density absorbers with the incidence of systems with log N(HI)≥21 decreasing for z $\gtrsim$ 3.5.

Acknowledgments

We would like to thank Bob Carswell for providing software for and assistance with the data reduction and profile fitting of the spectra. LSL acknowledges support from an Isaac Newton Studentship, the Cambridge Overseas Trust, and a University of California President's Postdoctoral Fellowship. RGM acknowledges the support of the Royal Society.

REFERENCES

Bahcall J.N., Peebles P.J.E., 1969, ApJ, 156, L7
Carswell R.F., Morton D.C., Smith M.G., Stockton A.N., Turnshek D.A., Weymann R.J., 1984, ApJ, 278, 486
Cooke A.J., 1994, Ph.D. Thesis. Cambridge University
Fall S.M., Pei Y.C., McMahon R.G., 1989, ApJ, 341, L5
Giallongo E., D'Odorico S., Fontana A., McMahon R.G., Savaglio S., Cristiani S., Molaro P., Trevese D., 1994, ApJ, 425, L1
Lanzetta K.M., Wolfe A.M., Turnshek D.A., 1995, ApJ, 440, 435
Lanzetta K.M., Wolfe A.M., Turnshek D.A., Lu L., McMahon R.G., Hazard C., 1991, ApJS, 77, 1
Lu L, Sargent W.L.W., Womble D.S., Barlow T.A., 1996, ApJ, 457, L1
Pei Y.C., Fall S.M., Bechtold J., 1991, ApJ,378, 6
Pei Y.C., Fall S.M., 1995, ApJ, 454, 69
Petitjean P., Webb J.K., Rauch M., Carswell R.F., Lanzetta K.M., 1993, MNRAS, 262, 499
Pettini M., Boksenberg A., Hunstead R.W., 1990, ApJ, 348, 48
Pettini M., Smith L.J., Hunstead R.W., King D.L., 1994, ApJ, 426, 79
Rauch M., Carswell R.F., Robertson J.G., Shaver P.A., Webb J.K., 1990, MNRAS, 242, 698
Sargent W.L.W., Steidel C.C., Boksenberg A., 1989, ApJS, 79, 703

Sargent W.L.W., Young P.T., Boksenberg A., Tytler D., 1980, ApJS, 42, 41
Schechter P., 1976, ApJ, 203, 297
Schechter P., Press W.H., 1976, ApJ, 203, 557
Stengler-Larrea E.A., et al., 1995, ApJ, 444, 64
Storrie-Lombardi L.J., McMahon R.G., Irwin M.J., Hazard C., 1994, ApJ, 427, L13 (Paper I)
Storrie-Lombardi L.J., McMahon R.G., Irwin M.J., Hazard C., 1996, ApJ, 468, 121 (Paper II)
Storrie-Lombardi L.J., McMahon R.G., Irwin M.J., 1996, MNRAS, in press (Paper IV)
Tytler D., 1987, ApJ, 321, 49
Wampler E.J., Williger G.M., Baldwin J.A., Carswell R.F., Hazard C., McMahon R.G., 1996, A&A, in press
Williger G.M., Baldwin J.A., Carswell R.F., Cooke A.J., Hazard C., Irwin M.J., McMahon R.G., Storrie-Lombardi L.J., 1994, ApJ, 428, 574
Wolfe A.M., 1987, Proc.Phil.Trans.Roy.Soc., 320, 503
Wolfe A.M., Turnshek D.A., Smith H.E., Cohen R.D., 1986, ApJS, 61, 249
Wolfe A.M., Lanzetta K.M., Foltz C.B., Chaffee F.H., 1995, ApJ, 454, 698

APPENDIX A: MAXIMUM LIKELIHOOD ANALYSIS

Using equation 5 for the column density distribution function, the damped Lyα absorbers will be found randomly distributed according to this function along the QSO line-of-sight in $N-z$ space. If the space is divided into m cells each of volume δv, the expected number of points in cell i is given by

$$\phi_i = f(N,z)_i \delta v. \tag{A1}$$

The probability of observing x_i points in cell i is

$$p(x_i) = e^{-\phi_i} \frac{\phi_i^{x_i}}{x_i!}. \tag{A2}$$

The likelihood function for QSO$_j$ taking the product over all the cells is then

$$L_j = \prod_{i=1}^{m} p(x_i) = \prod_{i=1}^{m} e^{-\phi_i} \frac{\phi_i^{x_i}}{x_i!}. \tag{A3}$$

If the volume of each cell δv becomes very small such that there is either 1 or 0 points in each cell,

$$x_i = \begin{cases} 1, & \text{if DLA detected;} \\ 0, & \text{if none detected,} \end{cases}$$

then the likelihood can be rewritten separating out the terms for full and empty cells. For $m = g$ empty cells + p full cells

$$L_j = \prod_{i=1}^{g} e^{-\phi_i} \prod_{j=1}^{p} e^{-\phi_j} \phi_j = \prod_{i=1}^{m} e^{-\phi_i} \prod_{j=1}^{p} \phi_j \tag{A4}$$

Taking the log of the likelihood function gives

$$\begin{aligned} \log L_j &= \sum_{i=1}^{m} -\phi_i + \sum_{j=1}^{p} \ln \phi_j \\ &= \sum_{i=1}^{m} -f(N,z)_i \delta v + \sum_{j=1}^{p} \ln f(N,z)_j + p \ln \delta v \end{aligned} \tag{A5}$$

(cf. Schechter & Press 1976). Ignoring the constant terms, in the limit where $\delta v \to 0$ this becomes

$$\begin{aligned} \log L_j &= -\int_{z_{min}}^{z_{max}} \int_{N_{min}}^{N_{max}} f(N,z) dN dz + \sum_{j=1}^{p} \ln f(N,z)_j \\ &= -\int_{z_{min}}^{z_{max}} \int_{N_{min}}^{N_{max}} k N^{-\beta} (1+z)^{\gamma} dN dz + \sum_{j=1}^{p} \ln\left[k N^{-\beta} (1+z)^{\gamma}\right] \end{aligned} \tag{A6}$$

To get the overall log likelihood for n QSOs we evaluate the integrals in equation A6 and additively combine the log L's resulting in

$$\begin{aligned} \log L &= \sum_{i=1}^{n} \Big[\frac{k N_{min}^{1-\beta}}{(1-\beta)(1+\gamma)} \Big((1+z_{em}^{i})^{1+\gamma} - (1+z_{min}^{i})^{1+\gamma} \Big) + p \ln k \\ &+ \sum_{j=1}^{p_i} \Big(-\beta \ln N_j + \gamma \ln(1+z_{dla}^{j}) \Big) \Big] \end{aligned} \tag{A7}$$

where p_i is the number of detected DLAs in QSO$_i$ and N_{min} is the minimum column density.

Figure 1. The profile fit and $\pm 1\sigma$ fits to the damped Lyα absorbers are shown as solid lines. The error arrays are shown as dotted lines. The components are listed in table 2. (a) The HI absorption complex in BR1033−0327 at z=4.15 is a system of at least 5 absorbers with a total column density of log $N_{\rm HI}= 20.15 \pm 0.11$ atoms cm^{-2}. (b) The damped Lyα absorber in BRI1108−0747 at z=3.607 with log $N_{\rm HI}= 20.33 \pm 0.15$ atoms cm^{-2}. (c) The damped Lyα absorber in BR1202−0725 at z=4.383. This is the highest redshift damped Lyα absorber known. The central damped component is shown with log $N_{\rm HI}$=20.49±0.15.

Figure 2. A single power law form of the column density distribution function, $f(N) = kN^{-\beta}$, fit to the entire damped Lyα sample from the APM Damped Lyα Survey, WTSC, LWTLMH, and LWT. The parameters of the fit are $\beta = 1.74$ and $\log k = 13.9$.

Figure 3. (a) The cumulative distribution for $17.2 \leq \log N_{\rm HI} \leq 22$. The stepped line is the data for all the damped Lyα systems in the data set. The circled point is the number of Lyman limit systems that would be expected given the redshift path covered in the damped Lyα surveys. In (b)-(d) the same distribution is overplotted with single power law fits for different values of β that were fit to the graph by eye. (b) shows that $\beta = 1.34$ will fit from the Lyman limit column density through the damped systems with log $N_{\rm HI} \approx 21$, a flatter slope than the canonical $\beta \approx 1.5 - 1.7$ range. (c) shows that $\beta = 1.69$ fits the systems with $20.3 \leq \log N_{\rm HI} \leq 21.2$ well but does not describe the high or low column density tails of the distribution. (d) shows a fit to the sharp drop off in numbers of damped systems with log $N_{\rm HI} \gtrsim 21$. This is evident from just looking at the estimated column densities for the damped systems in table 3 or by looking at the spectra. There are not a lot of heavily damped systems.

Figure 4. The cumulative HI column density distribution with the sample split in half at $z = 2.5$. The damped Lyα systems with $z > 2.5$ are shown by the solid line and the absorbers with $z < 2.5$ are shown by the dashed line. The higher redshift absorbers appear to have a slightly flatter slope up to log $N_{\rm HI}$= 21 and then a sharper drop in the number of very high column density systems, though a K-S test shows that this is not a statistically significant difference.

Figure 5. The log column density distribution function $f(N)$ vs. the log column density $N_{\rm HI}$ plotted over 4 redshift ranges, z=[0.008, 1.5], [1.5, 2.5], [2.5, 3.5], and [3.5, 4.7], all binned in the column density ranges log $N_{\rm HI}$=[20.3, 20.5], [20.5, 21.0], and [21.0, 21.8]. The gradual flattening of the distribution function from redshift z=0 to z=3.5 is evident. The most striking feature is the steepness of the distribution in the highest redshift bin. It is not just steeper due to a decrease in the highest column density systems (log $N_{\rm HI}$>21), but there is also an increase in the number of lower column density systems.

Figure 6. (a)The log-likelihood function for the Γ-distribution form of the column density distribution function, $f(N, z) = (f_*/N_*)(N/N_*)^{-\beta} exp(-N/N_*)$. The >68.3%, >95.5%, and >99.7% confidence contours are plotted for log N_* and β. The best fit values are log $N_* = 21.63$, $\beta = 1.48$, and $f_* = 1.77 \times 10^{-2}$ which is solved for analytically. (b) The Γ-distribution function, $f(N, z) = (f_*/N_*)(N/N_*)^{-\beta} exp(-N/N_*)$, overplotted on the differential form of the column density distribution. The fit is to the entire data set including the surveys from Paper II, WTSC, LWTLMH, and LWT. The parameters for the fit are log $N_* = 21.63$, $\beta = 1.48$, and $f_* = 1.77 \times 10^{-2}$. (c) The cumulative distribution for $17.2 \leq$ log $N_{\rm HI} \leq 22$ as shown in figure 3(a) is now overplotted with the Γ-distribution form of the column density distribution function. The dashed line now clearly fits the entire distribution for log $N_{\rm HI}$≥20.3. The circled point is again the number of Lyman limit systems that would be expected given the redshift path covered in the damped Lyα surveys. This is not included in the fit.

Figure 7. This figure shows the same data plotted in figure 6 but the fit includes the expected number of Lyman limit systems, given the redshift path surveyed. (a) The log-likelihood function for the Γ-distribution form of the column density distribution function, $f(N, z) = (f_*/N_*)(N/N_*)^{-\beta} exp(-N/N_*)$. The >68.3%, >95.5%, and >99.7% confidence contours are plotted for log N_* and β. The best fit values are log $N_* = 21.36$, $\beta = 1.16$, and $f_* = 4.43 \times 10^{-2}$ which is solved for analytically. (b) The Γ-distribution function, $f(N, z) = (f_*/N_*)(N/N_*)^{-\beta} exp(-N/N_*)$, overplotted on the differential form of the column density distribution. The fit is to the entire data set including the surveys from Paper II, WTSC, LWTLMH, and LWT. The parameters for the fit are log $N_* = 21.36$, $\beta = 1.16$, and $f_* = 4.43 \times 10^{-2}$. (c) The cumulative distribution for $17.2 \leq$ log $N_{\rm HI} \leq 22$ overplotted with the Γ-distribution form of the column density distribution function. The circled point is again the number of Lyman limit systems that would be expected given the redshift path covered in the damped Lyα surveys.

Figure 8. The >68.3% and >95.5% confidence contours for the log-likelihood function are plotted for the number density per unit redshift of the damped absorbers. The best fit for a single power law form $N(z) = N_0(1+z)^\gamma$ yields $\gamma = 1.3 \pm 0.5$ and $N_0 = .04^{+.03}_{-.02}$ over the redshift range 0.008 < z < 4.7.

Figure 9. The number density of DLA per unit redshift, $N(z)$, vs. z(absorption). The dashed bins show N(z) for all the damped systems and the solid bins for systems with N(HI)≥ 10^{21} atoms cm^{-2}. A single power law fit of N(z)= $.04(1+z)^{1.3}$ is overplotted. This is consistent with no intrinsic evolution in the absorbers even though the value of γ is similar to that found for the Lyman limit systems where evolution is detected at a significant level (Paper I).

Figure 10. The HI column density of the damped Lyα absorbers is plotted versus absorption redshift. The paucity of absorbers with log $N_{\rm HI}$> 21 at z > 4 is apparent.

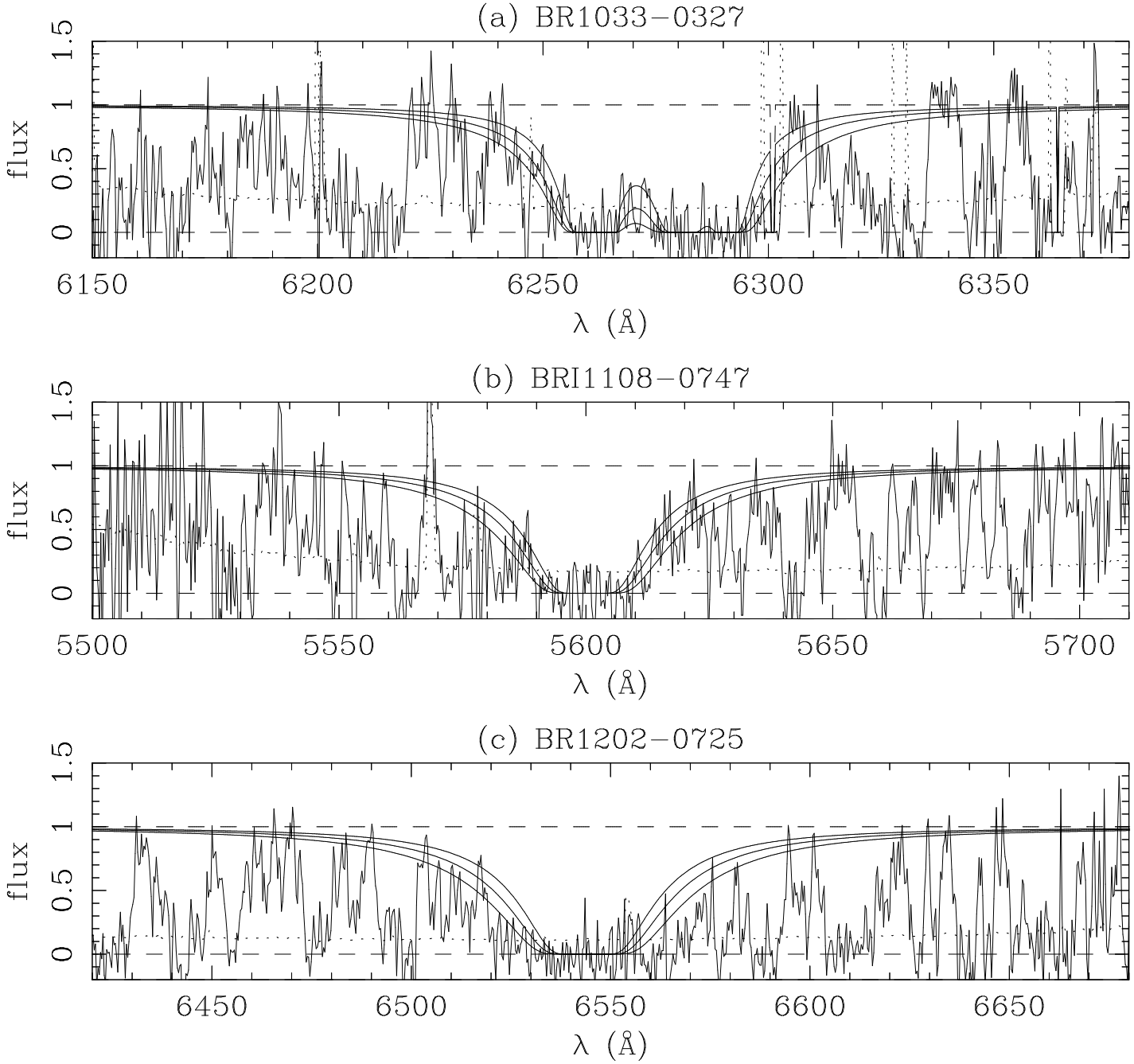
(a) BR1033−0327
flux
0
0.5
1
1.5
6150
6200
6250
6300
6350
λ (Å)
(b) BRI1108−0747
flux
0
0.5
1
1.5
5500
5550
5600
5650
5700
λ (Å)
(c) BR1202−0725
flux
0
0.5
1
1.5
6450
6500
6550
6600
6650
λ (Å)

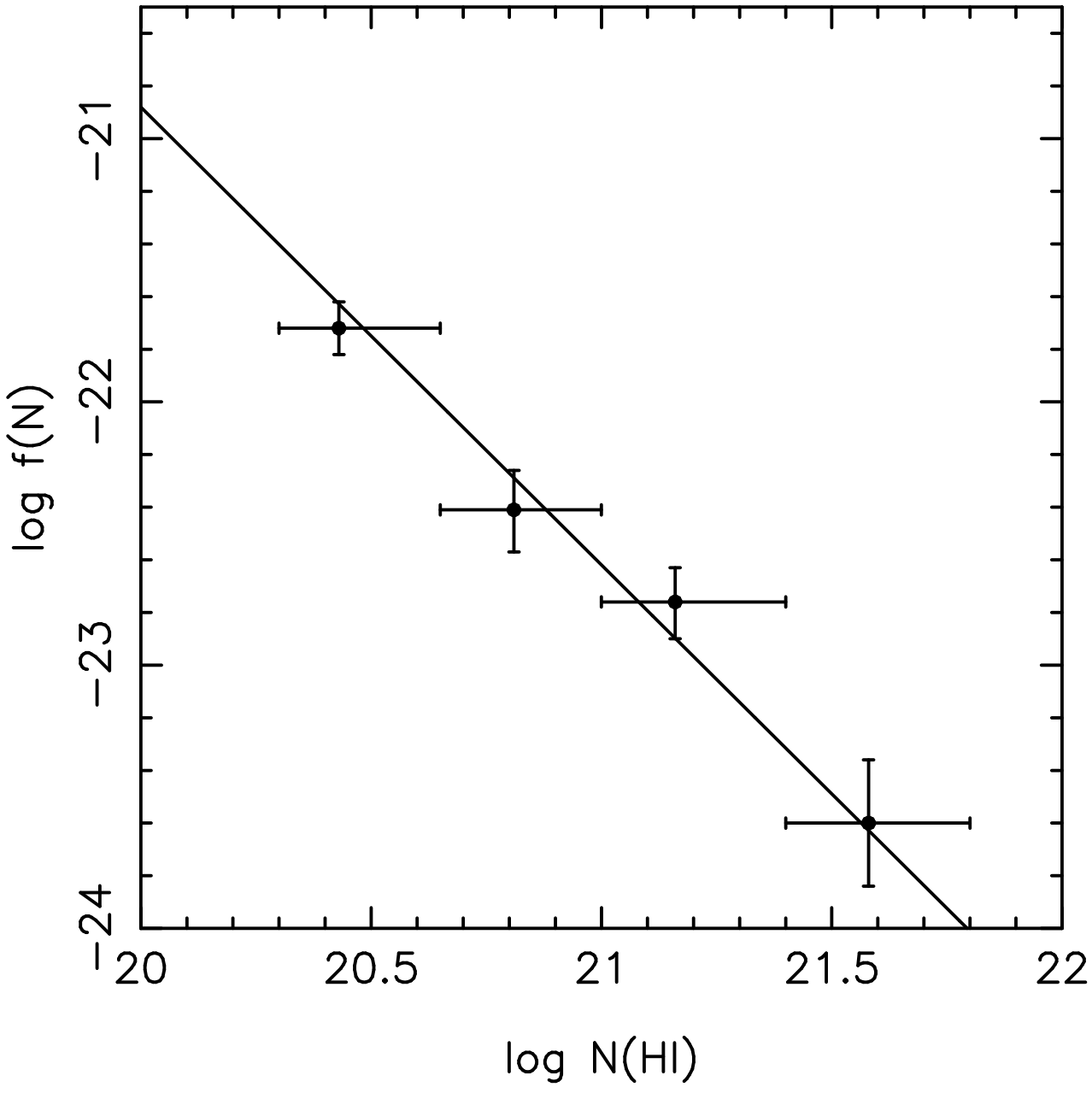
log f(N)
−21
−22
−23
−24
20
20.5
21
21.5
22
log N(HI)

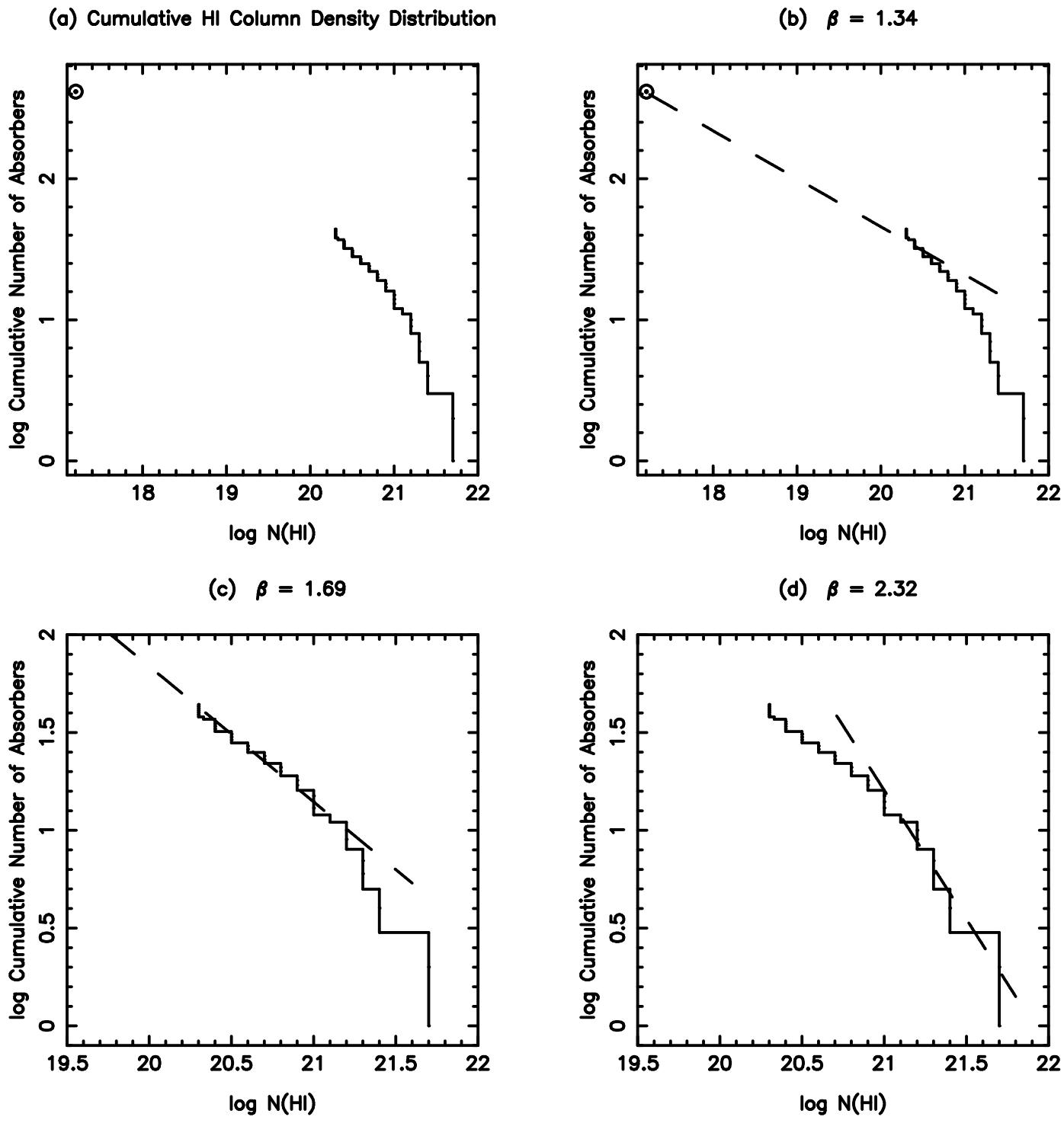
(a) Cumulative HI Column Density Distribution
(b) β = 1.34
(c) β = 1.69
(d) β = 2.32
log Cumulative Number of Absorbers
log N(HI)
0
0.5
1
1.5
2
18
19
20
21
22
19.5
20
20.5
21
21.5

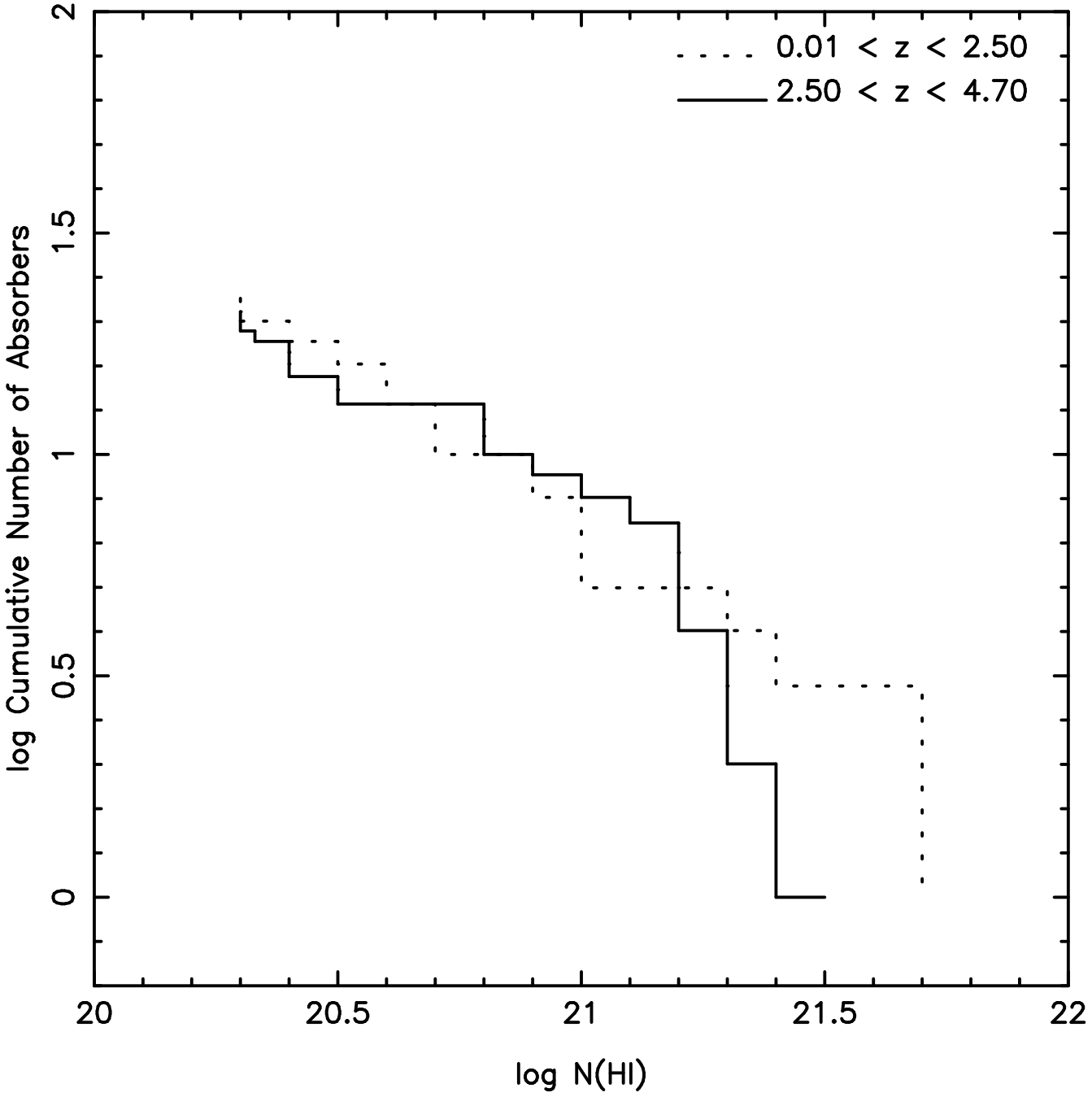
0.01 < z < 2.50
2.50 < z < 4.70
log Cumulative Number of Absorbers
log N(HI)
0
0.5
1
1.5
2
20
20.5
21
21.5
22

.008 ≦ z < 1.5

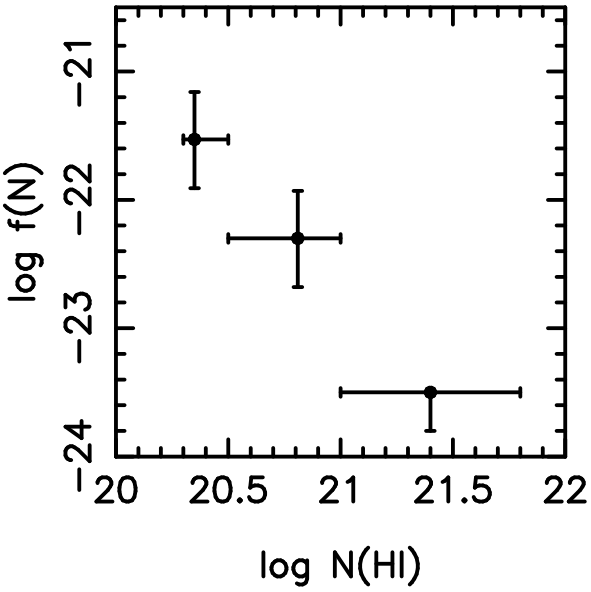

1.5 ≦ z < 2.5

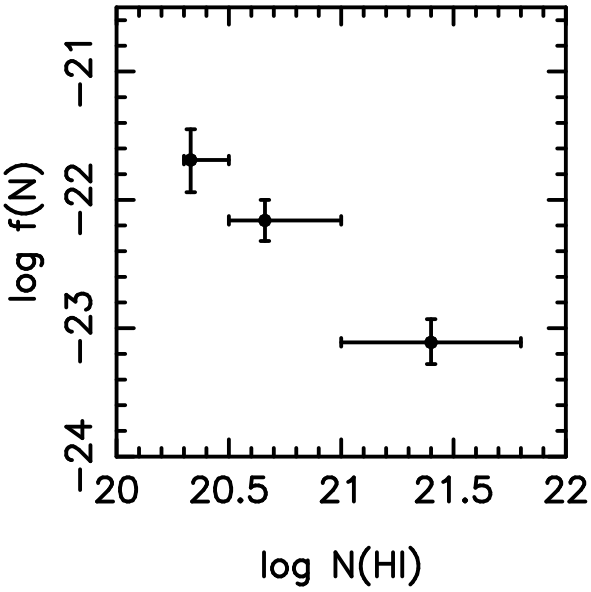

2.5 ≦ z < 3.5

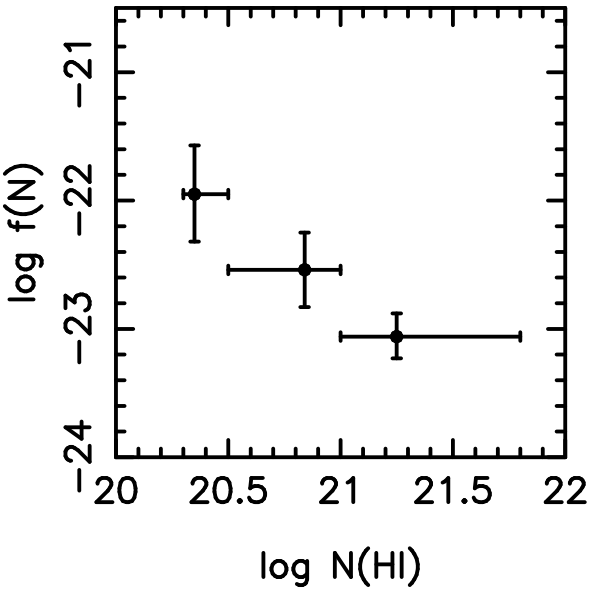

3.5 ≦ z < 4.7

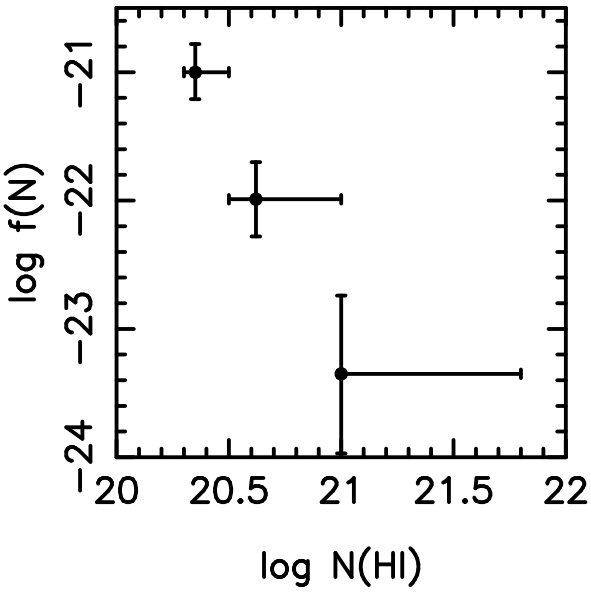

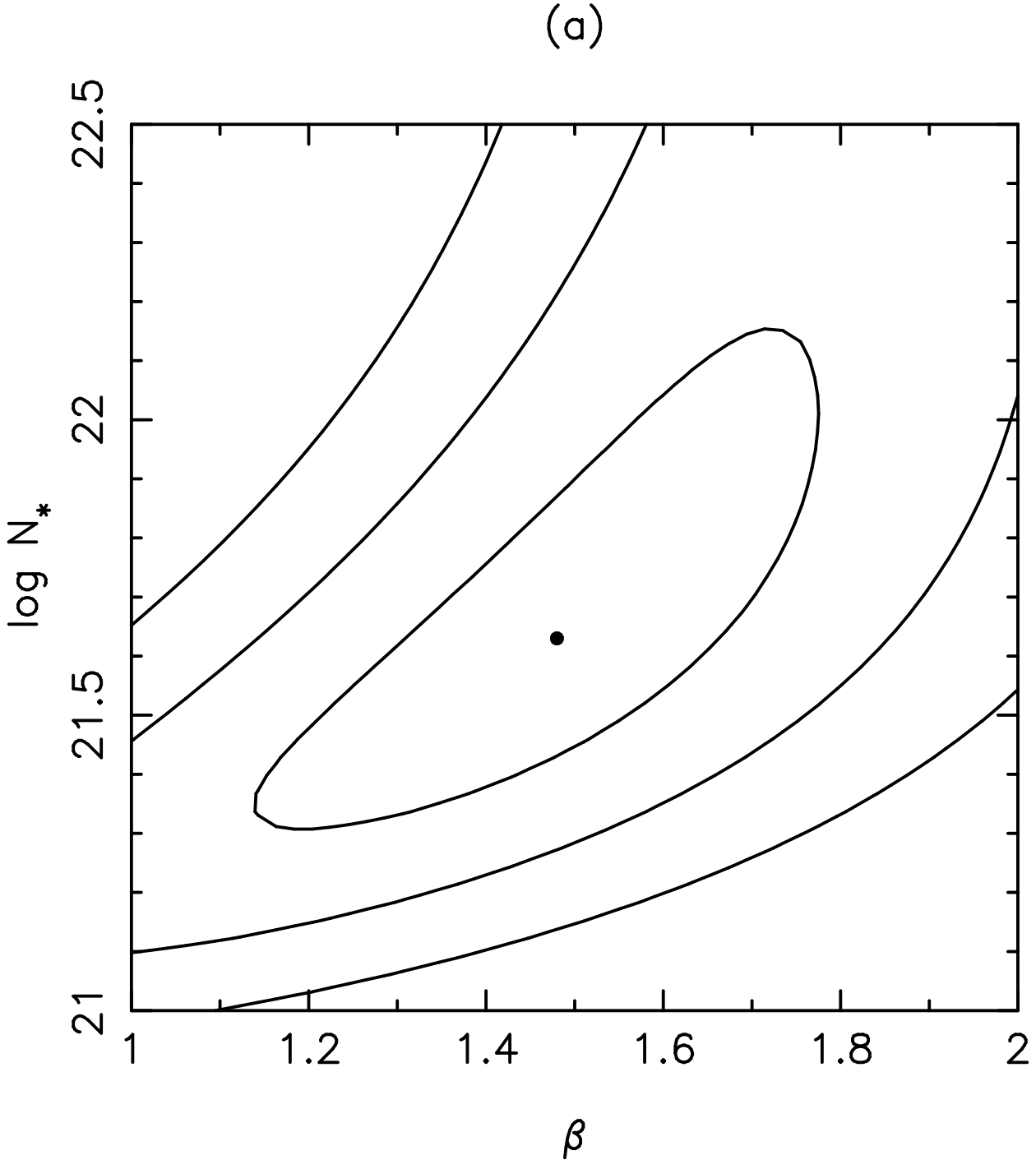
(a)
log N*
22.5
22
21.5
21
1
1.2
1.4
1.6
1.8
2
β

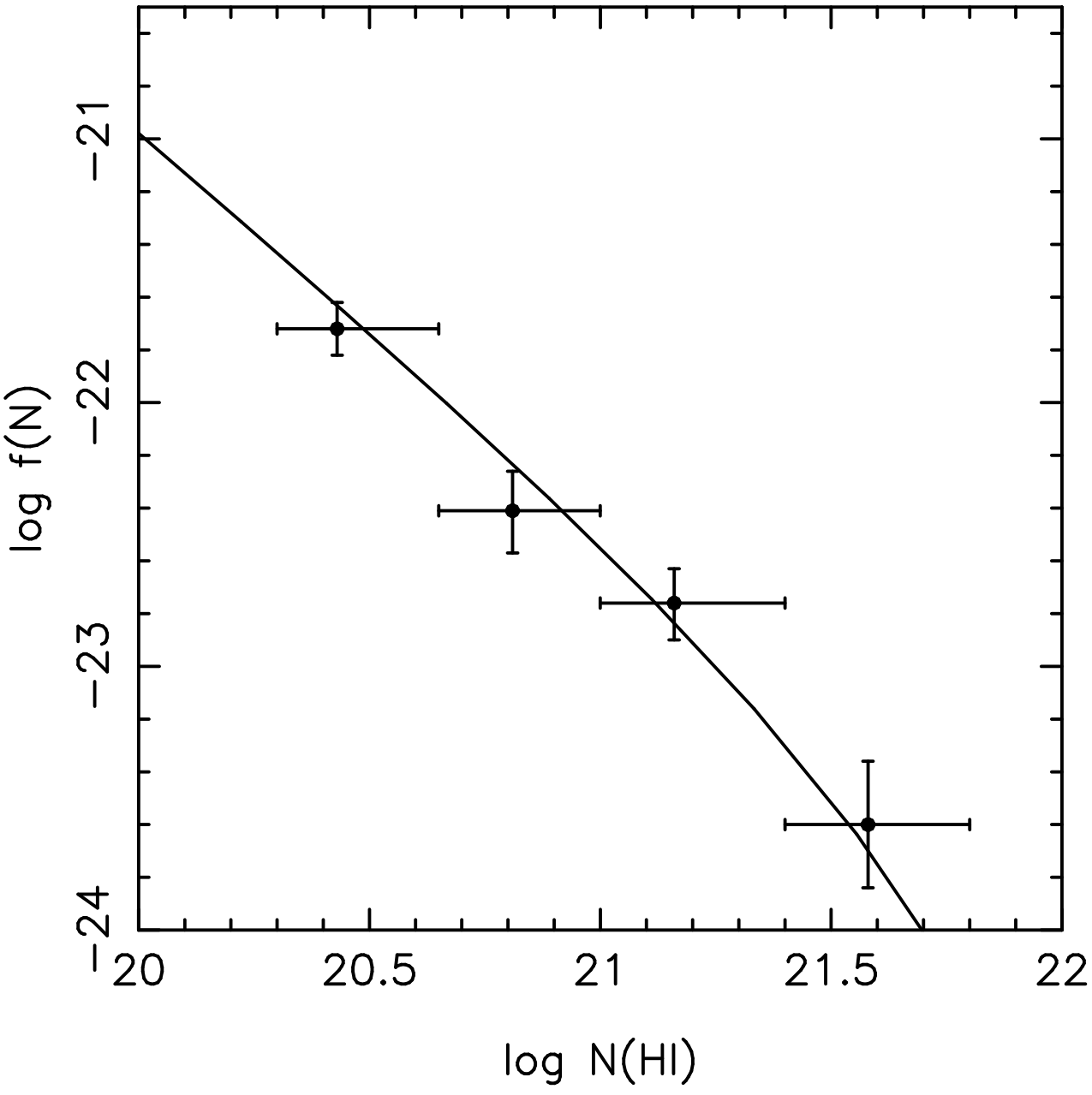
log f(N)
−21
−22
−23
−24
20
20.5
21
21.5
22
log N(HI)

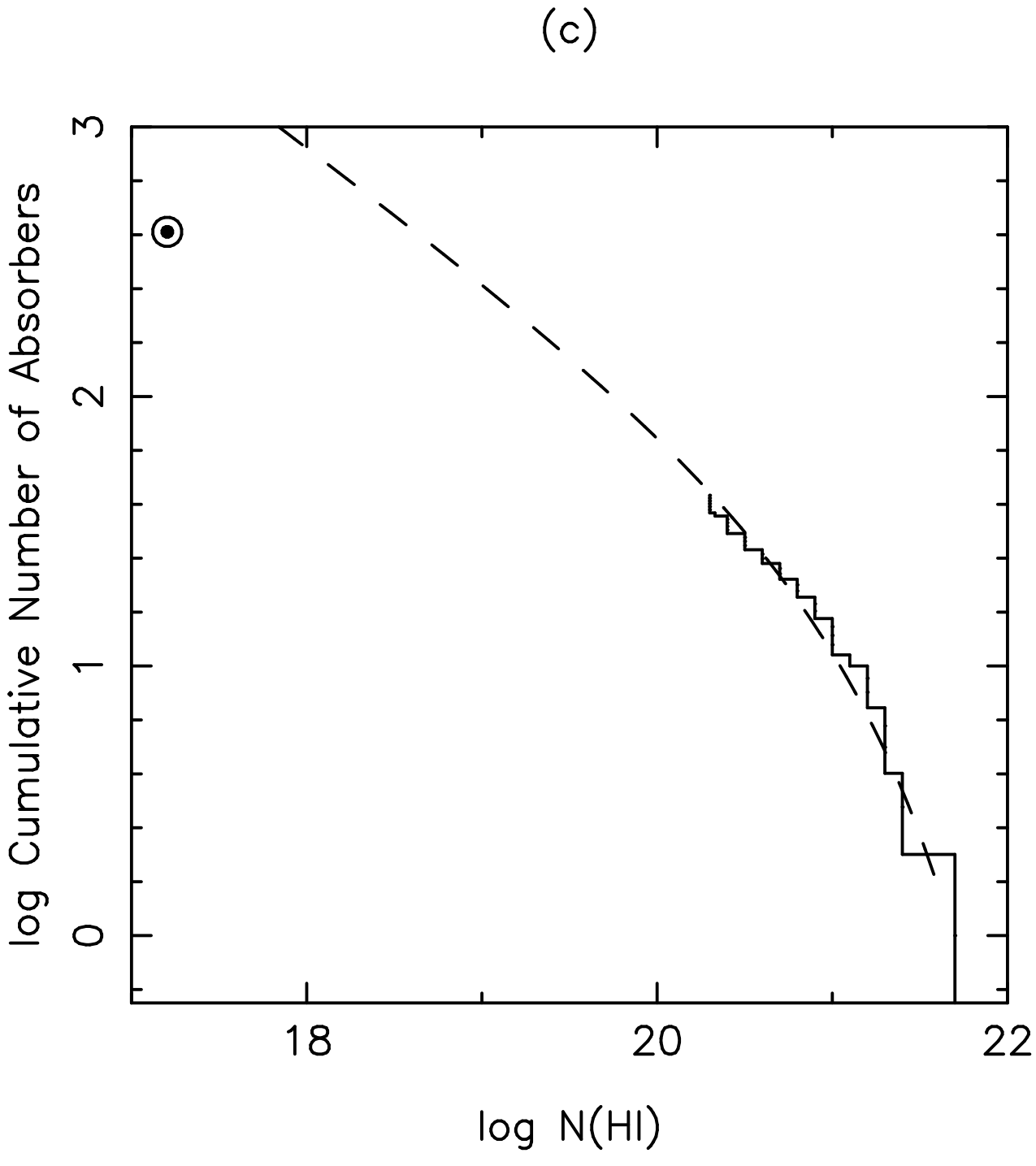
(c)
log Cumulative Number of Absorbers
0
1
2
3
18
20
22
log N(HI)

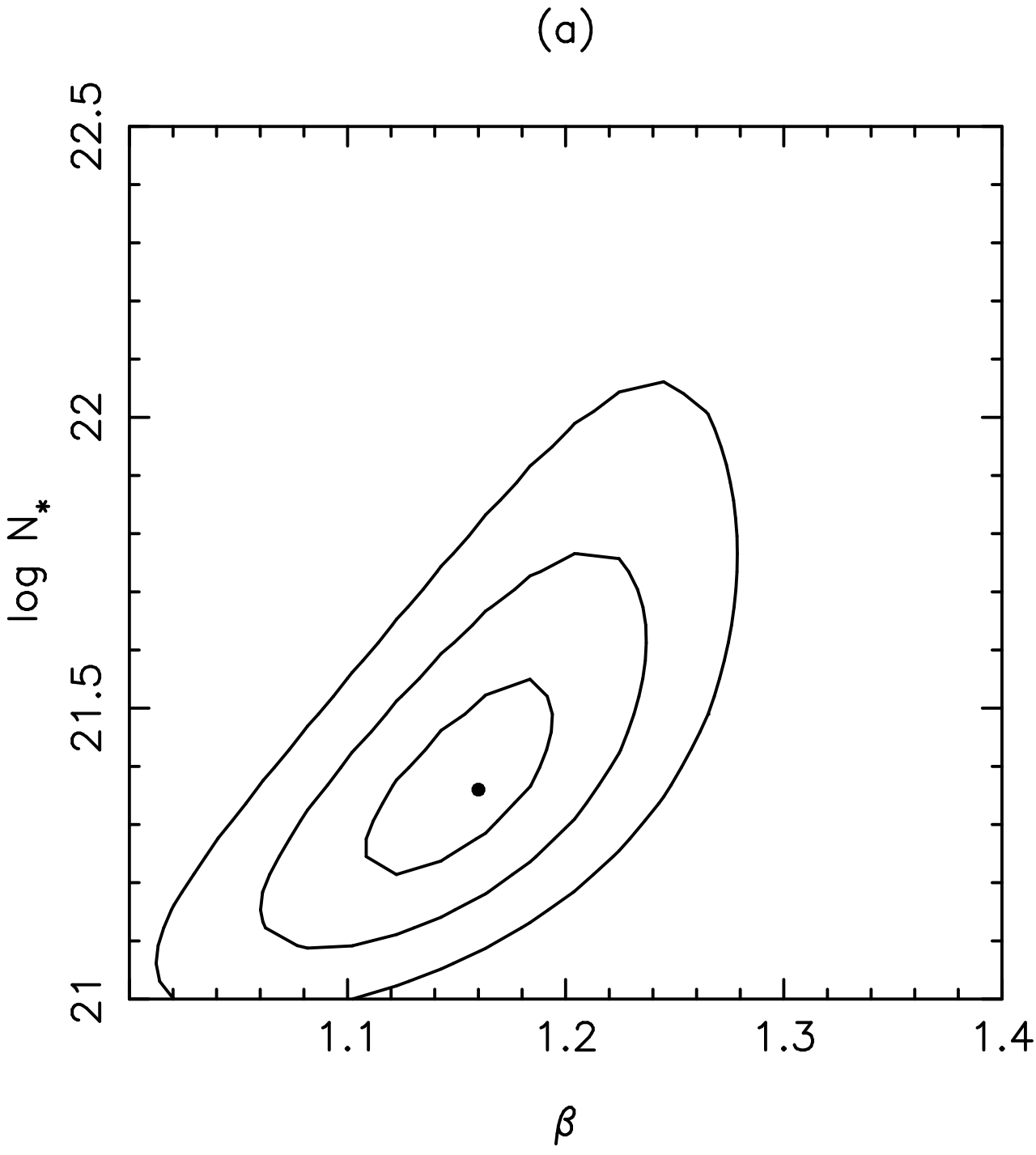
(a)
22.5
22
21.5
21
log N*
1.1
1.2
1.3
1.4
β

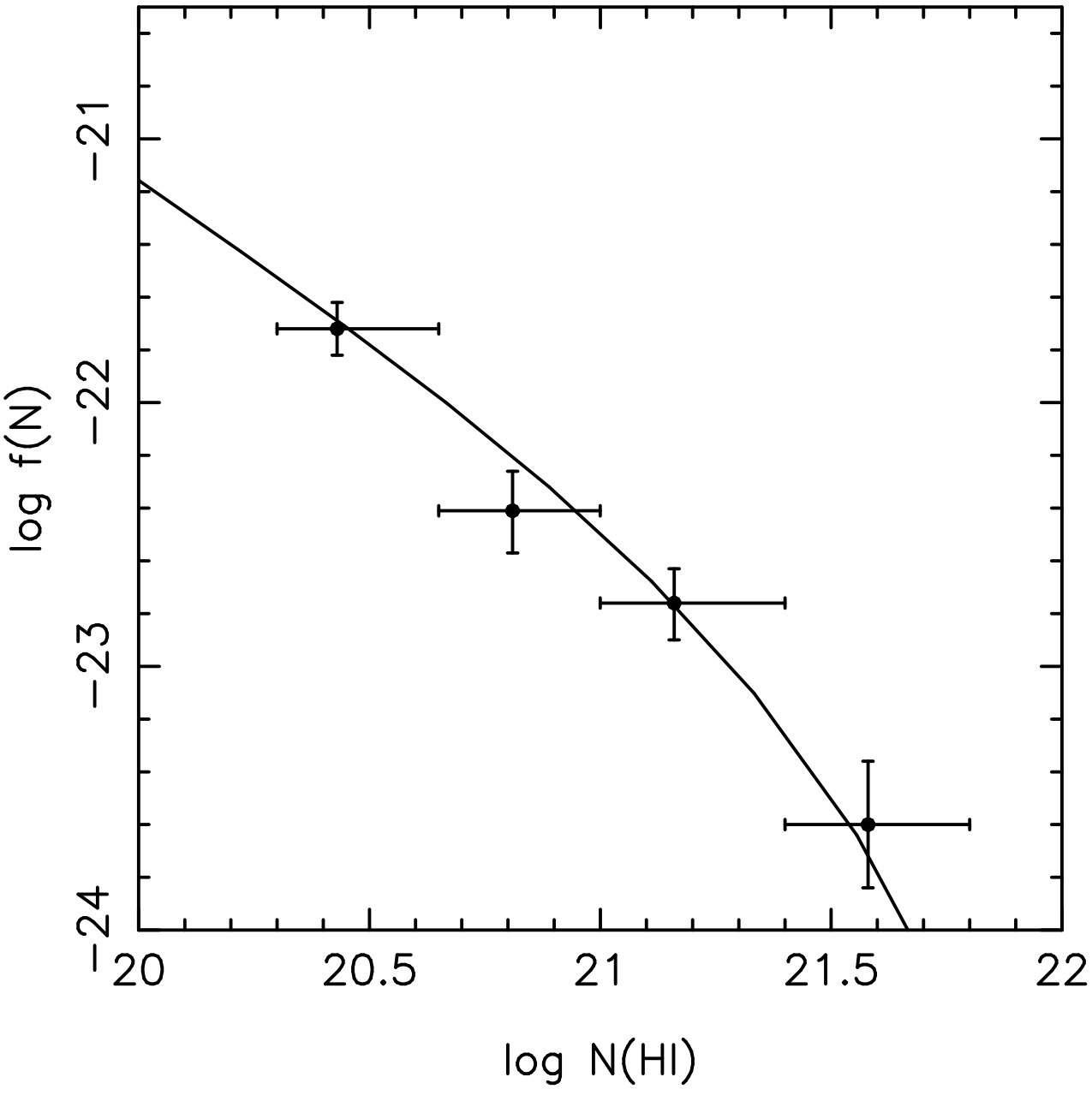
log f(N)
−21
−22
−23
−24
20
20.5
21
21.5
22
log N(HI)

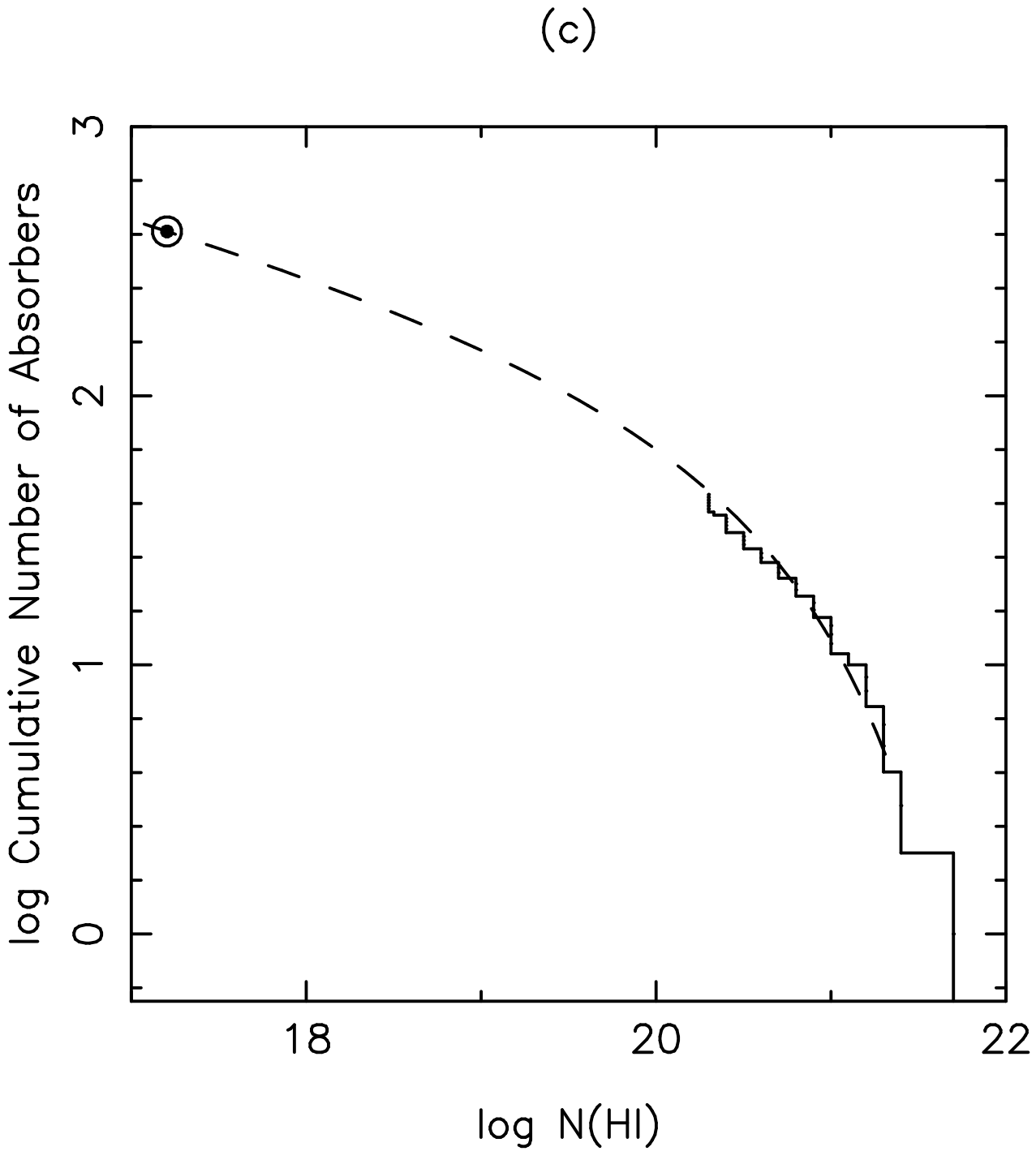
(c)
log Cumulative Number of Absorbers
0
1
2
3
18
20
22
log N(HI)

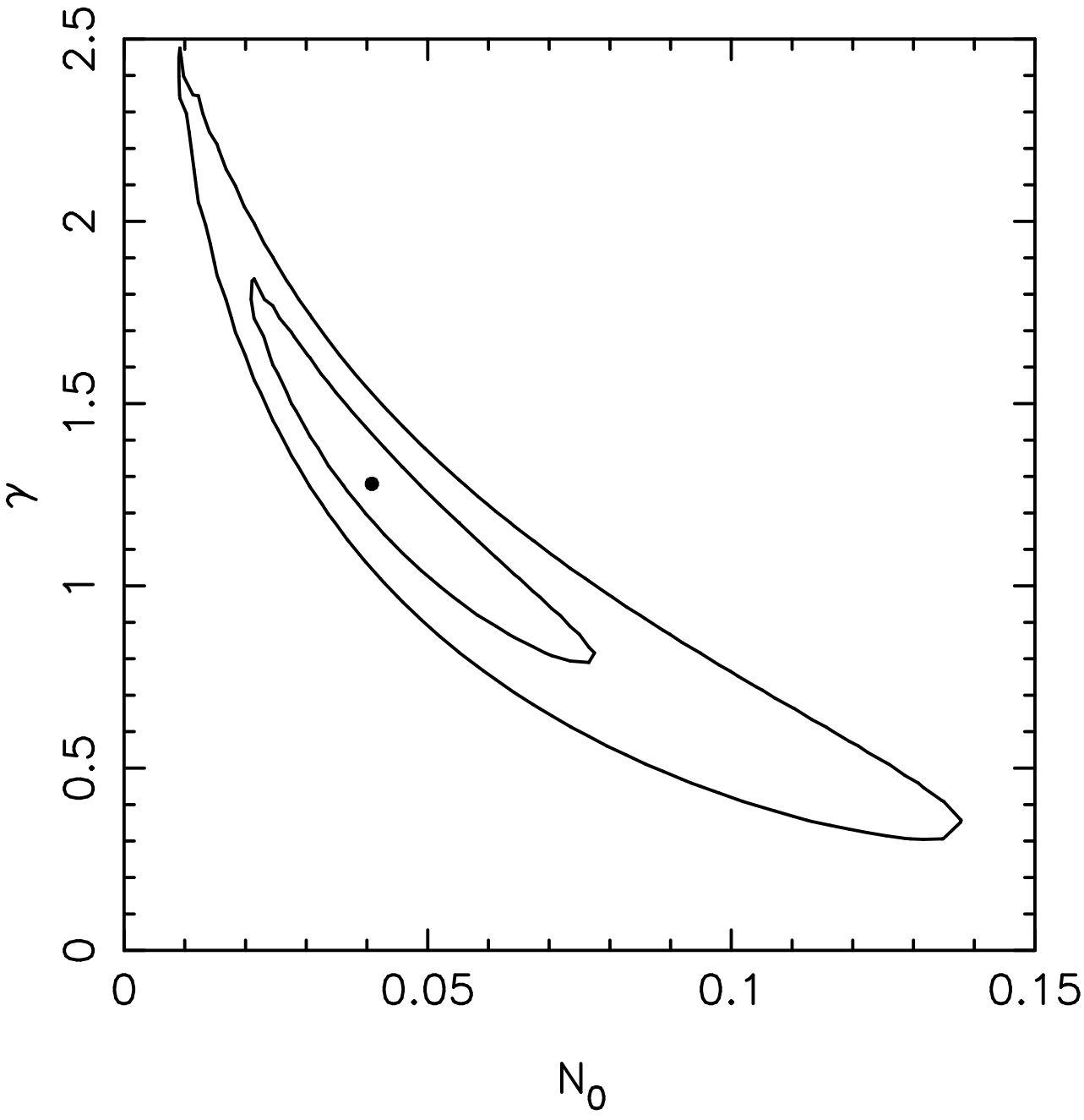
2.5
2
1.5
1
0.5
0
γ
0
0.05
0.1
0.15
N0

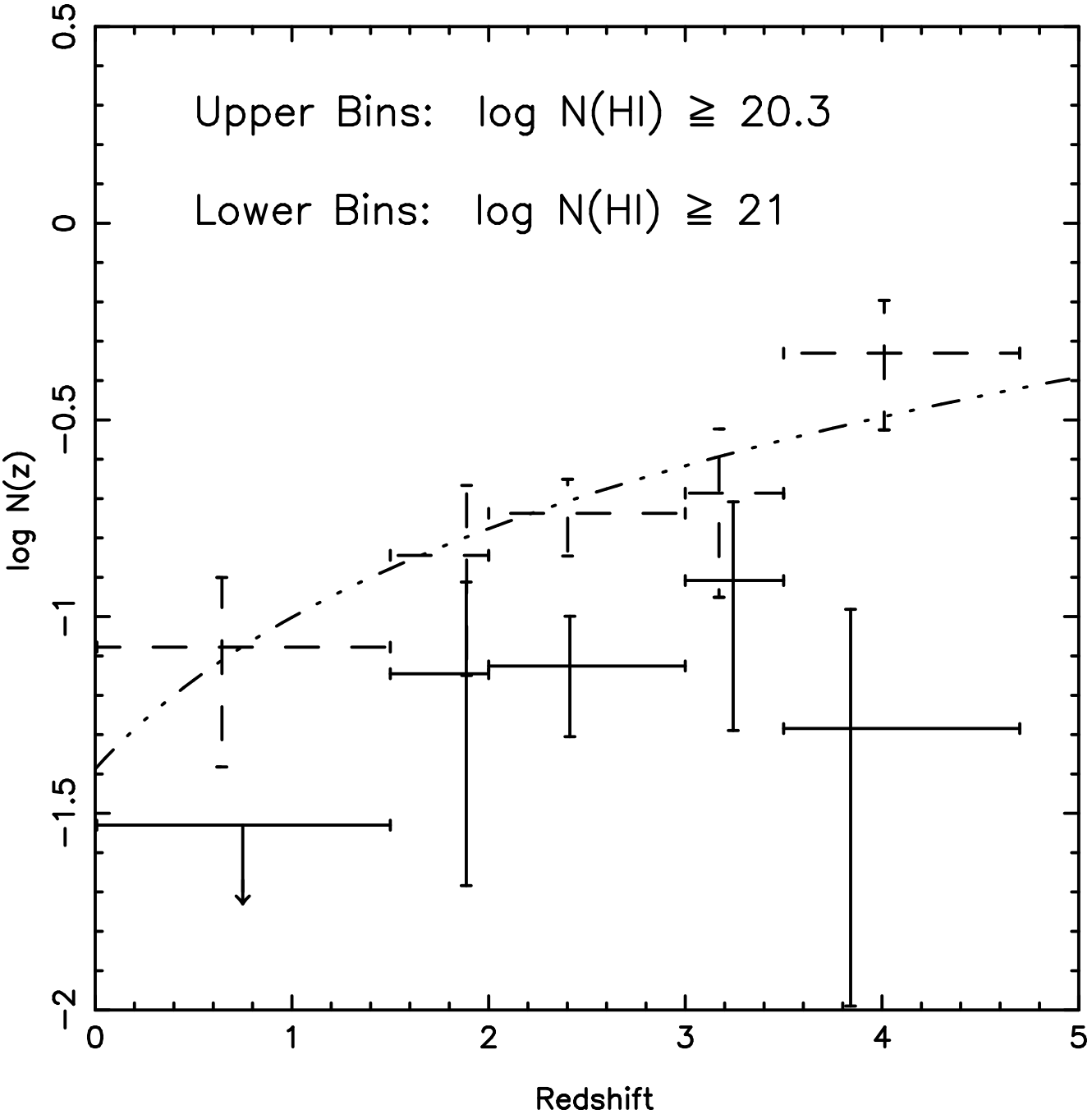
Upper Bins: log N(HI) ≧ 20.3
Lower Bins: log N(HI) ≧ 21
log N(z)
Redshift
0.5
0
−0.5
−1
−1.5
−2
0
1
2
3
4
5

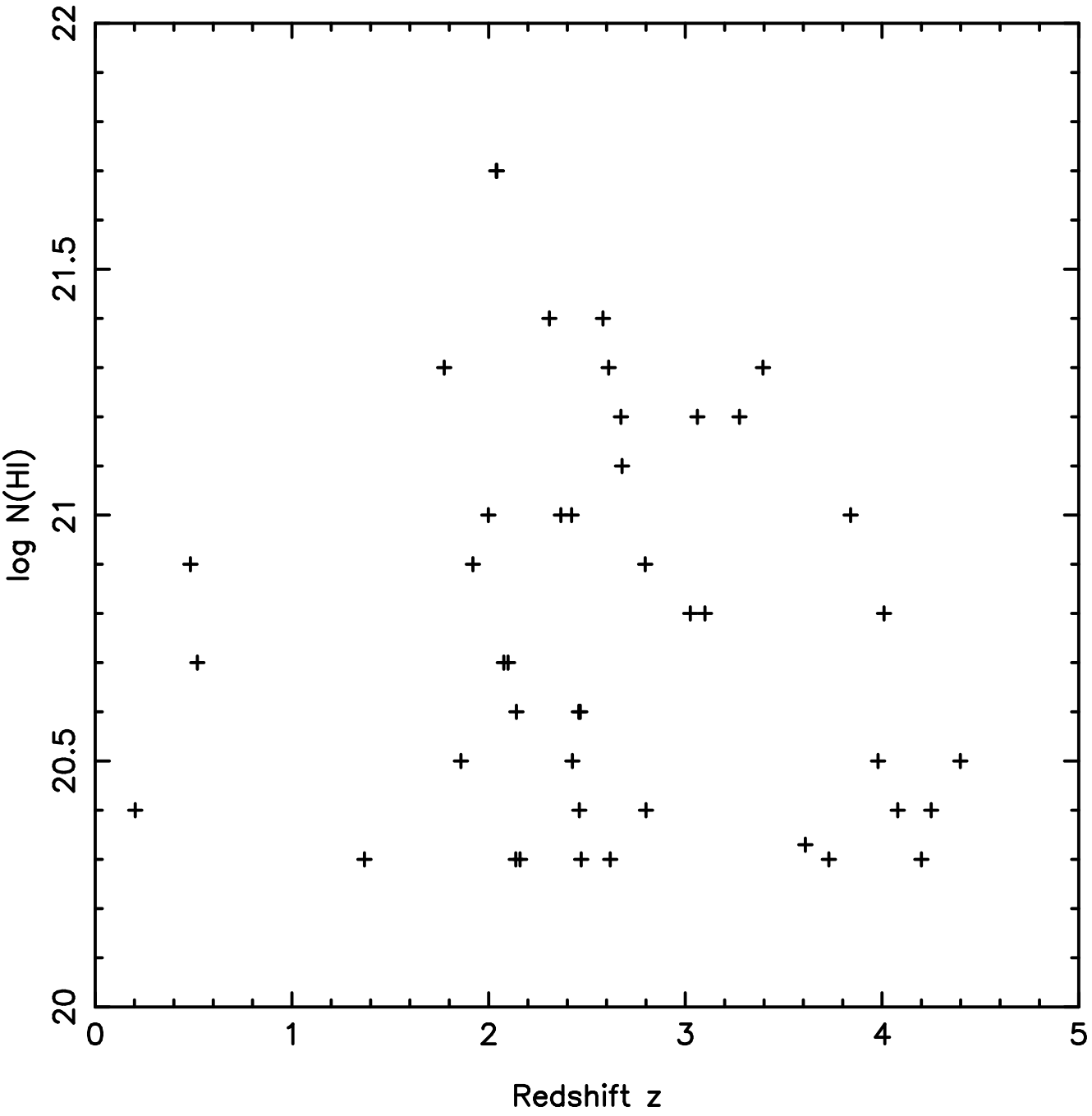
log N(HI)
22
21.5
21
20.5
20
0
1
2
3
4
5
Redshift z